



Enhanced stability during reduction of stratification in the North Sea

Hans van Haren^{a,*}, M.J. Howarth^b

^aDepartment of Physical Oceanography, Royal Netherlands Institute for Sea Research (NIOZ), P.O. Box 59, Den Burg 1790 AB, The Netherlands

^bProudman Oceanographic Laboratory, Joseph Proudman Building, 6 Brownlow Street, Liverpool L3 5DA, UK

Received 3 February 2003; received in revised form 10 December 2003; accepted 30 January 2004

Abstract

In summer shelf seas are (increasingly with time) stably stratified in density due to solar heating. Previous observations have shown that this stratification may become marginally stable when increased stratification is accompanied by enhanced vertical current differences ('shear') that de-stabilize the water column. When the effects of shear become larger than those of stratification, so that the gradient Richardson number $Ri < 1$, mixing may result, most likely by the (occasional) overturning at the layer of strong shear to the point of breaking of short high-frequency internal waves that propagate through the stratification. The shear is dominantly at the low-frequency end of the internal gravity wave band, the local inertial frequency. In autumn the accepted view is that stratification is reduced not only due to internal mixing following enhanced inertial shear, but also due to cooling by the atmosphere and wind mixing. However, in the present paper detailed observations from the northern North Sea clearly demonstrate for the first time that also in autumn periods of *increasing* stability with time occur. Furthermore, it is shown that enhanced stability may be a prerequisite for generating large amplitude high-frequency internal waves that may eventually break: autumn storms can first *reduce* inertial shear magnitude, followed by a new equilibrium of marginal stability across a layer of greatly reduced thickness. Such a thin, super-stable ($Ri \gg 1$) layer is then moved vertically by high-frequency (interfacial) internal waves. This 'creates' a background of reduced large-scale stratification, associated with the reduced inertial shear.

© 2004 Elsevier Ltd. All rights reserved.

Keywords: Pycnocline stability; High-frequency internal waves; Northern North Sea; 59°N01°E

1. Introduction

Classically, the gradual increase of density with depth becomes concentrated in a layer of enhanced vertical stratification (the 'pycnocline') at some

depth below the surface, beneath a near-homogeneous ('mixed') layer caused by atmospheric-induced mixing (Munk and Anderson, 1948). Stable density stratification limits turbulent mixing and hence further deepening of the pycnocline by mechanical processes. Externally governed pycnocline erosion has been studied since the pioneering work of Ekman who showed that the Earth's

*Corresponding author.

E-mail address: hansvh@nioz.nl (H. van Haren).

rotation controls the ocean's response to wind stress: the (well-mixed) Ekman layer of (spiraling) current shear stress above the pycnocline. Pollard et al. (1973) showed that Ekman layer (and pycnocline) deepening following an increase in wind stress stops after one inertial period. A typical depth for an Ekman layer is several tens of metres, which is comparable to the depth of a near-surface mixed layer caused by (night-time) convective cooling (Brainerd and Gregg, 1995).

In shelf seas, pycnocline deepening may be arrested by (tidal) shear stress from below, resulting in an extremely sharp pycnocline near mid-depth (Figs. 1a, b (i); Turner, 1973). In addition, Turner and Krauss (1967) argue that pycnocline deepening can depend on the Richardson number, defined by them as the ratio between parameters involving stratification and the eroding turbulent friction velocity. Such eroding turbulence usually comes from external sources like atmospheric disturbances or bottom friction, but can be generated internally as well. The effects of external and internal erosion processes are easily recognizable in density-depth-time plots: external erosion reduces overall density differences across a pycnocline, while internal mixing does not, in the absence of other processes. In this paper we interpret turbulence within a pycnocline as an internal turbulent erosion (mixing) process and, following Turner (1973), we pursue some mechanisms behind it (Fig. 1b (ii)–(iii)).

In autumn in the Baltic, Krauss (1981) observed the importance of an internal mixing process in the erosion of the pycnocline from its thickening, caused by transient 'inertial' currents following the passage of an atmospheric disturbance. He modelled the process using time-dependent Ekman solutions. Similar indications of the importance of inertial currents on pycnocline erosion were found throughout the seasonal cycle of stratification in the central North Sea, in spring (van Haren, 2000), summer (van Haren et al., 1999) and autumn (van Haren, 1996).

Inertial currents are very sensitive to turbulent viscosity (Maas and van Haren, 1987), and have the peculiar behaviour of only being generated because of the reduced level of turbulent viscosity within the pycnocline, so that the weakly stratified

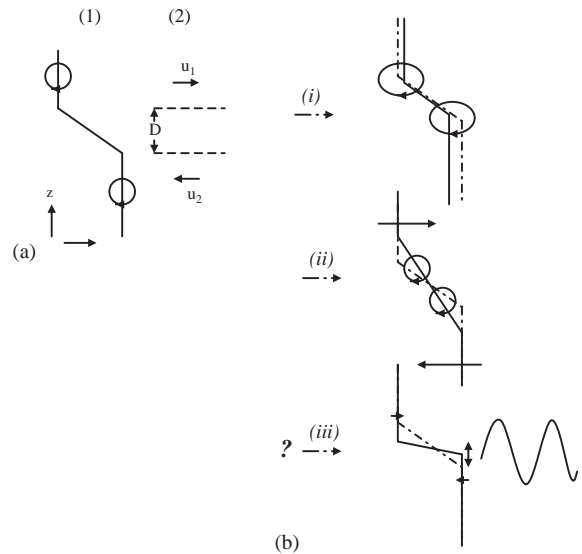


Fig. 1. Conceptual models of pycnocline stability and erosion governed by external and internal mixing processes (see also Fig. 4.19 in Turner, 1973). Currents are indicated by horizontal arrows, turbulence by closed ellipses. (a) Initial state of the summer-time stratification (1) with a single pycnocline and equally thick (D) shear layer (2) between frictional layers above and below. (b) This state (a; here dashed) is either modified to state (i) by penetrating (eroding) external turbulence reducing the pycnocline thickness and overall density difference without changing the density gradient, or to state (ii) representing the effects of internal mixing induced by enhanced shear across a layer of increased thickness and associated thickening of the pycnocline, following the breaking of high-frequency waves generated by the shear (Thorpe, 1971), thereby reducing stratification but not the overall density difference. The main question in this paper concerns whether state (iii) can be reached through an internal "mixing" process, commencing with a pycnocline of reduced thickness but enhanced stratification (due to unchanged overall density difference) under reduced shear and, subsequently, supporting large high-frequency internal waves that eventually break after interaction with the large scale shear.

near-surface layer acts like a slab (Pollard and Millard, 1970). As a result, large inertial current differences ('shear') are observed across the pycnocline, which may become de-stabilized locally (Fig. 1b (ii)). Such 'dynamical stability' of a water column is measured by the gradient Richardson number,

$$Ri(z, t) = \frac{N^2}{|S|^2}, \quad (1)$$

the square of the ratio of the buoyancy frequency, N , given by

$$N(z, t) = \left(-\frac{g}{\rho} \frac{d\rho}{dz} \right)^{0.5} \quad (2)$$

for density (ρ) and acceleration of gravity (g), and the magnitude $|\mathbf{S}|$ of de-stabilizing vertical current shear vector,

$$|\mathbf{S}|(z, t) = \left(\frac{\partial u}{\partial z}, \frac{\partial v}{\partial z} \right) \quad (3)$$

with u, v denoting the horizontal current components. Indeed, Krauss (1981) observed low-gradient Richardson numbers $Ri \sim 0.5$, corresponding to ‘marginally dynamic stability’, which varied only slowly with time (van Haren et al., 1999). This Ri -value is above the critical value for linear stability of small disturbances ($Ri = 0.25$), but below the value $Ri = 1$ for ‘formal stability’ considering three-dimensional nonlinear stratified flows (Miles, 1987). Munk (1981) suggested that as a result of this constantly low Ri the spectrum of internal waves, supported by the stratification, was saturated. van Haren et al. (1999) suggested that this expressed an interaction between the shear of low-frequency (near-inertial) waves generated by atmosphere (and tidal shear) and dissipation via the breaking of high-frequency internal waves near the buoyancy frequency. Such interaction between low-frequency shear and high-frequency internal waves was suggested from laboratory experiments (Thorpe, 1971), from open ocean thermocline observations (Marmorino, 1987; Marmorino et al., 1987) and from numerical modelling (Bouruet-Aubertot and Thorpe, 1999). Thus for internal mixing to occur (Fig. 1b (ii)) de-stabilizing shear interacts with internal waves first.

In the relatively shallow central North Sea, shear across stratification capping the bottom boundary layer is also at the dominant semidiurnal tidal frequency. Close to the bottom the shear magnitude and Ri vary on the tidal time scale. However, at the bottom of the pycnocline tidal shear has the same property as inertial shear: both are circularly polarized irrespective of the polarization of their currents, so that their shear magnitude varies over a much larger time scale

than the current components (van Haren, 2000). At some distance off the bottom, vertical tidal current variations are entirely governed by only one (the clockwise) of the two circular rotary components into which a tidal current ellipse can be decomposed. As a result, tidal shear across stratification exists following Ekman dynamics of frictionally modified barotropic currents, not because of internal tides (Maas and van Haren, 1987; van Haren, 2000).

Conceptually, the ‘constant’ internal shear-stratification ratio may become disturbed in two ways. Firstly, when stratification is weakened for a given shear, mixing increases, thereby further destabilizing stratification. Secondly, the opposite occurs when shear is decreased for fixed stratification, so that internal mixing decreases and further stabilization is expected.

In this paper observations are presented that clearly show that the latter process of enhancement of stratification can also occur counter-intuitively in the presence of autumn storms in the northern North Sea (Fig. 1b (iii)). It will also be shown that this ‘super-stability’ ($Ri \gg 1$) eventually also can lead to mixing. The results will be generalized by comparison with data from the shallower central North Sea, also during autumn.

2. Data

In the North Sea halfway between northern Scotland and southern Norway at $59^{\circ}20'N$, $01^{\circ}00'E$ (Fig. 2; $H = 110$ m water depth; maximum M_2 current amplitude 0.20 m s $^{-1}$) we deployed a 150 kHz RDI-broadband Acoustic Doppler Current Profiler (ADCP) in a sea bed frame for a period of 2 months. For details of all moorings see Howarth et al. (2002). The ADCP sampled 10 min average currents in 22 vertical bins of 4 m each from 11 m above the bottom upwards. Simultaneously, a standard Aanderaa thermistor string with 11 thermistors, resolving the water column around mid-depth at 5 m intervals sampling every 5 min, low-pass filtered to hourly values, was moored 5 km due east of the ADCP. In late October, between days 294.6–307.6, during

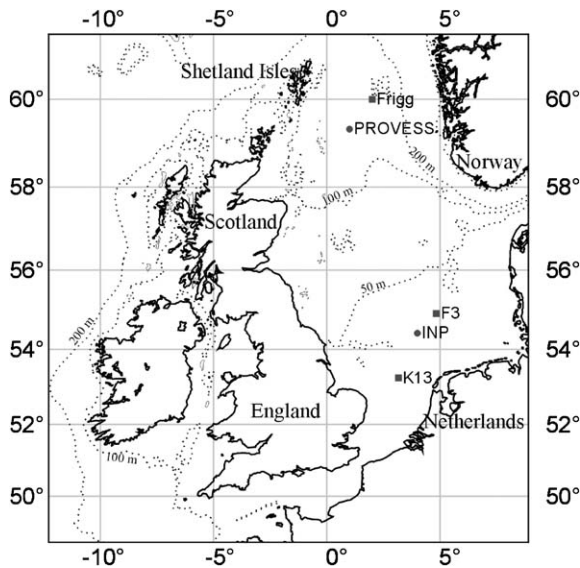


Fig. 2. Map of the North Sea showing the PROcesses of Vertical Exchange in Shelf Seas (PROVCESS) northern mooring site and the nearby Frigg oil rig at which meteorological data were collected. For comparison, some data from the central North Sea (mooring site INP) will be analysed in the Section 6 with meteorological data from rigs K13 and F3.

the last 2 weeks of their deployment detailed temperature measurements were made using a specially designed thermistor string (van Haren et al., 2001) at 1.3 km due north of the ADCP. This ‘fast thermistor string’ held 32 sensors evenly spaced at 1 m intervals. The sensors had a response time $\tau < 0.25$ s, they were sampled once every 30 s and had a relative accuracy better than 0.5 mK.

Prior to deployment of the thermistor strings, Seabird SBE-911 CTD information was obtained at 24 Hz, resolving almost the entire water column while being lowered typically at 1.0 m s^{-1} . This information was used to determine the depth of the pycnocline (Fig. 3 in Knight et al., 2002) and the thermistor strings were subsequently moored so that they covered the pycnocline in the upper section of their range. We expected the pycnocline to descend with progressive near-surface mixing. In retrospect, this expectation was wrong, especially for the deployment of the fast thermistor string, and the pycnocline ascended

with time, despite mixing events. CTD-information obtained (only) during the first week of deployment of the fast thermistor string established the relationship,

$$\delta\rho = -(0.25 \pm 0.02)\delta T \quad \text{for 42 profiles} \\ \text{between days 290–300} \quad (4)$$

with salinity, similarly two-layered, contributing a fair amount to density variations. This relationship was used to compute N in Eq. (2) using thermistor string data.

Adopting the viewpoint that N determined the wave-guide for internal waves in a WKB-sense, so that the vertical scale of N was much larger than the wave amplitude, averaging over the pycnocline thickness gave typical values of $N = 1 - 3 \times 10^{-2} \text{ s}^{-1}$ in the pycnocline. (We use $1 \text{ s}^{-1} = 1 \text{ rad s}^{-1} = 86,400/2\pi \text{ cpd.}$) As a result, the sampling strategy of the fast thermistor string was adequate (Nyquist frequency $\sigma_{\text{Nyq}} = 1.05 \times 10^{-1} \text{ s}^{-1}$). As we demonstrate below, higher frequency internal waves at very small scales were only just resolved by the fast thermistor string, while not being resolved by the standard thermistor string and ADCP. We used the fast thermistor string data to estimate vertical length scale variations of stratification. Standard thermistor string and ADCP data were used to estimate ‘background’ Richardson number variations on the larger scales (5 m in the vertical; 30 min in time).

Some information on turbulent diffusivity was obtained from 42 raw CTD-profiles obtained within 2 km from the moorings between days 290–300. Following Thorpe (1987),

$$K = 0.15d_s^2 N, \quad (5)$$

where d_s is the displacement scale, the depth scale over which an instability has to be displaced to obtain a ‘re-ordered’ entirely static stable density profile. As N was extremely difficult to estimate properly in weakly stratified surface and bottom boundary layers, Eq. (5) was only used to estimate K across a pycnocline using a condition $N > N_m$, an (arbitrary) minimum value. Meteorological data were obtained from the Frigg oil field ($59^\circ 54' \text{N}$, $02^\circ 06' \text{E}$).

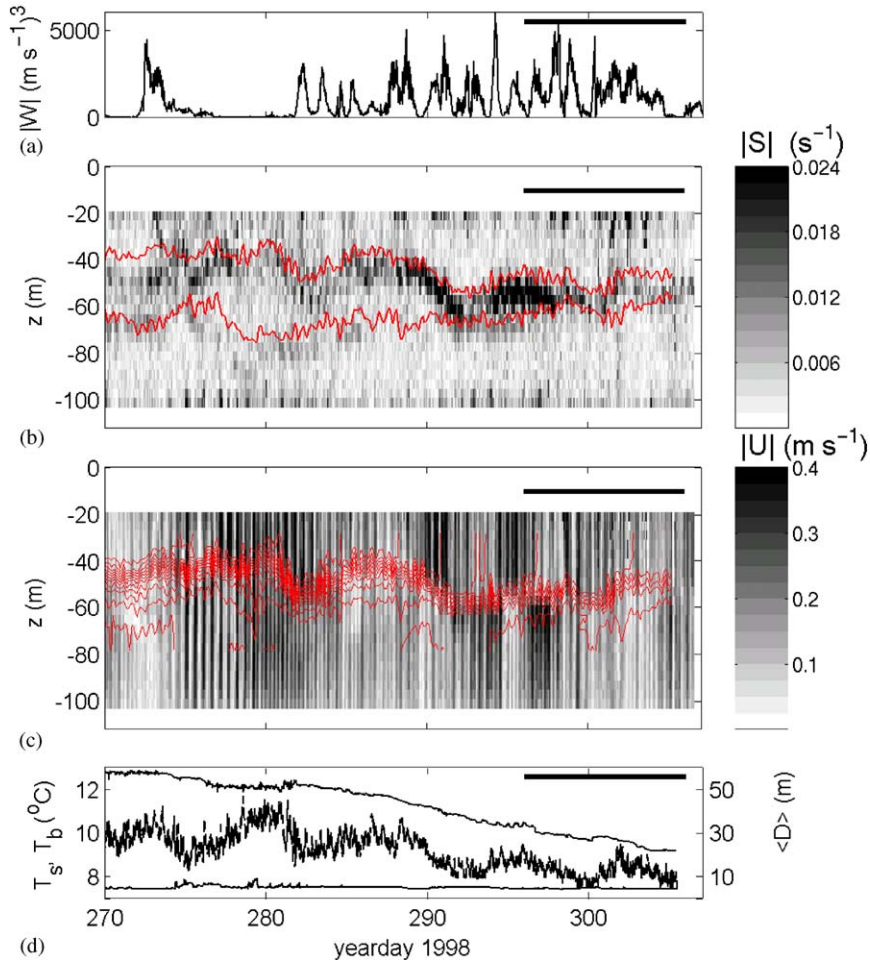


Fig. 3. Overview of current shear and stratification observed in the northern North Sea in October, 1998. Time is given in yeardays, according to the convention that yearday 1.5 = 12.00 UTC at January 1. (a) Wind speed (cubed) measured at Frigg. (b) Current shear magnitude $|S| = ((\Delta u/\Delta z)^2 + (\Delta v/\Delta z)^2)^{0.5}$ computed from $\Delta z = 4$ m bins data from the bottom-mounted 150 kHz ADCP. Solid red lines indicate the smoothed depth and height of the near-surface (z_s) and -bottom (z_b) layers in Eq. (6), respectively, from 5 m thermistor string data on a mooring 5 km east of the ADCP mooring. (c) Current magnitude from the ADCP. Solid red lines indicate smoothed temperature contours between 7.5° and 12.5°C at 0.5°C intervals. (d) Temperature measured at 30 (upper solid line) and 107 m depth (lower line) and hourly filtered pycnocline thickness D , defined in Eq. (6), (middle line; scale to the right). In each panel, the thick horizontal bar indicates the period of detailed observations.

3. General observations of a pycnocline in autumn

During 2 months of observations the reduction of stratification was observed in different ways, although not before day 270, the end of September (Fig. 3). The surface temperature remained constant until about October 1 (yearday 274), after that decreasing with time due to atmospheric-induced mixing and surface heat loss. The near-

bottom temperature initially increased very slowly with time (at most by 0.15°C over 30 days), but after day 280 it remained constant or even decreased slightly. This indicated that exchange with warmer near-surface waters probably did not occur during that period. There was some uncertainty in this lack of exchange across the pycnocline, as changes in the vertical distribution produced by horizontal advection of horizontal

temperature could be mistaken for vertical heat exchange. Modelling efforts by Burchard et al. (2002) showed large buoyancy fluxes across the sea surface having little effect on diapycnal exchange. Nevertheless, large activity (discussed in Sections 4 and 5) was observed near and in the pycnocline for which horizontal advection was not important.

Assuming a constant Ri (van Haren et al., 1999; van Haren, 2000), we represented the location and strength of stratification by the value of ($\Delta z = 4$ m, $\Delta t = 10$ min)-shear (Fig. 3b). The depth of the ‘pycnocline’ thus estimated varied little with time and remained between about 40 and 60 m depth. (Other methods for estimating the pycnocline gave similar values, see for instance Knight et al., 2002, Fig. 11.) These depths were still far above the computed tidal bottom boundary layer, extending 20–30 m above the bottom for an observed amplitude of 0.20 m s^{-1} for M_2 and 0.07 m s^{-1} for S_2 . The tidal bottom boundary layer dominated the observed (total current) bottom boundary layer progressively less with time (Knight et al., 2002). Thus, the practical pycnocline thickness D is defined as

$$D(t) = z_s - z_b \quad (6)$$

with

$$z_s = z(|T - T_s| > TD, t),$$

$$z_b = z(|T - T_b| < TD, t)$$

using an (arbitrary) threshold of $TD = 0.1^\circ\text{C}$. D was relatively thick albeit varying with time (Fig. 3d) for hourly smoothed temperatures T_s and T_b are inferred from measurements (once per 5 min) at the upper and lower thermistor of the standard thermistor string, respectively. On the large time scale of weeks, this D decreased with time like the overall temperature difference. On smaller time scales of a few days, D varied with wind stress input (Fig. 3a). We attributed the rather surprising thickening of the near-bottom boundary layer above the tidal frictional height to two effects, both being in response to atmospheric forcing (Appendix A). In later analysis of the pycnocline using unsmoothed high-resolution thermistor string data D is defined using $TD = 0.4^\circ\text{C}$ ($\Delta\rho \sim 0.1 \text{ kg m}^{-3}$).

Apart from some near-surface shear caused by wind stress in the second half of the record, shear was largest near mid-depth. Its value increased by at least a factor of two during a short period between days 261 and 265 (van Haren et al., 2003), and again between days 287 and 297 (Fig. 3b). During these periods enhanced inertial motions were observed (Fig. 3c). This was observed from the modulation of near-surface and, in anti-phase across the pycnocline, of near-bottom currents, which had a period of about 4.5–5 days. The beat period between f and M_2 is 4.77 days. This observed pattern of inertial-tidal modulation was similar to that observed in the central North Sea in summer (van Haren et al., 1999), including the strong mode-1 appearance of the inertial motions (the tidal currents being mainly barotropic). The amplitude A_f of near-inertial currents was again just less than that of the local barotropic semidiurnal tidal currents ($A_f/A_{M_2} \approx 0.7$). At the depth of the pycnocline the inertial frequency strongly dominated the shear signal (Knight et al., 2002; van Haren et al., 2003), which showed circular anti-cyclonic polarization implying a magnitude that varied on a much larger time-scale than an inertial period. Inertial shear was abruptly generated within an inertial period (van Haren, 2000) like inertial motions (Pollard and Millard, 1970; Millot and Crépon, 1981).

With the focus on inertial current generation sudden attenuation of inertial shear is perhaps less well studied. We investigated in some detail the period between days 294.6 and 306, which includes the largest inertial currents and shear and their sudden collapse (Fig. 3b and c), due to a wind stress change in anti-phase with the near-surface inertial motion when an atmospheric disturbance passed (Knight et al., 2002). It will be shown that large wind stress not always leads to stratification erosion, but occasionally to enhanced pycnocline stability due to such loss of diapycnal shear.

4. Collapse of inertial shear

Sudden changes in stratification following a change in shear on day 298 (Fig. 3) was observed in detail in different ways: in current observations,

in kinetic energy spectra, in potential energy spectra, and in CTD and thermistor string observations, as will be demonstrated below.

In depth-time, the transition in stratification was visible from the decrease of the pycnocline thickness, thereby increasing its magnitude (Figs. 4 and 5). After day 298, N was coloured progressively darker red in Fig. 4d. In the detail plots of Fig. 5 the thermocline thinning is clearly visible. This was not observed in the coarse low-pass filtered data from the standard thermistor string in Fig. 3c and d ($\Delta z = 5$ m; $\Delta t = 60$ min). The thinner pycnocline of enhanced stratification also occasionally showed enhanced vertical excursions with an estimated amplitude increase by a factor of up to 1.5 (Figs. 4d and 5a,b). These changes in stratification and the largest pycnocline excursions followed *after* a sudden reduction in shear (Figs. 3b and 4b,c), which cannot be attributed to inadequate resolution of vertical scales (shear was computed using 4 m vertical increments, whereas temperature in Figs. 4 and 5 was sampled every 1 m). Not only the shear magnitude decreased, but also the current difference across the pycnocline regardless of changes in thickness (Fig. 4b). This current difference between near-surface and -bottom boundary layers (mainly induced by mode-1 inertial motions; Fig. 3c) reduced by a factor of 0.45 ± 0.05 . A change of similar amount was observed in 5 days mean stratification, which is not so easily visible in Figs. 4 and 5 (which suggest an increase in stratification with time). As day 300 delineated the most distinct transition in stratification (Fig. 6), two averaging periods A and B of equal (5 days) length were chosen, somewhat arbitrarily. It is noted that the average value for N_A computed between days 294.6–298.0 was the same as computed for the 5-day period 294.6–299.6. Only the standard deviation was different, as is obvious in Fig. 6b.

Indeed the maximum N -value per profile of unsmoothed thermistor string data increased between days 298 and 300.5 (Fig. 6a). During the same period, stratification changed in two ways at the depths of the pycnocline (Fig. 6b). From its average (days 294.6–299.6) ‘single-valued’ level of $N_A = 2.4 \pm 0.6 \times 10^{-2} \text{ s}^{-1}$, N adopted a new equilibrium at two levels between days 300.50 and

305.5: $N_B \approx 1.1 \pm 0.3 \times 10^{-2} \text{ s}^{-1}$ and, during short periods of time, much larger values of $N_{00} \approx 4.8 \times 10^{-2} \text{ s}^{-1}$ (maximum value observed around $z = -59$ m: $N_{00} = 6.5 \times 10^{-2} \text{ s}^{-1}$). As a result

$$N_B/N_A = 0.45 \pm 0.1, \quad (7)$$

well within the error bounds similar to the drop in current difference across the pycnocline. Within the period B, the short-term N_{00} -periods were accompanied by an enhancement of temperature ‘noise’ (Fig. 6c). We inferred that this indicated internal wave activity at increased frequencies and mixing in the presence of *enhanced* static stability. This temperature noise was not white noise, as we observed in (potential energy) spectra discussed below.

The averaging periods A and B were also chosen as large as possible to have maximum spectral resolution and statistical significance. The spectra from the two periods showed distinct changes, in contrast with the observed enhanced stability (N_{00}) but confirming the observed decrease in 5 days average stratification $N_A \rightarrow N_B$ (Fig. 7). In potential energy spectra $P_{PE}(\sigma) = 0.5N^2P_\eta(\sigma)$, inferred from isotherm displacement spectra $P_\eta(\sigma)$ interpolated from high-resolution temperature observations within the pycnocline, we observed a shift of the spectral enhancement near the buoyancy frequency towards lower frequency, more or less by amount (7). Meanwhile, for $\sigma \ll N$ the level of this spectrum dropped, again more or less by the factor in Eq. (7), while the kinetic energy spectrum $P_{KE}(\sigma)$ of currents observed above (or below) the depth of the pycnocline also decreased by a factor of ~ 0.4 for $\sigma \gg f$ (Fig. 7). As a result, both energy spectra confirmed the reduction in observed *large-scale* (> 4 m vertical scale, > 1 day averaging) stratification

$$P_B(\sigma)/P_A(\sigma) \propto N_B/N_A \approx 0.45. \quad (8)$$

Both (independent) sets of current and temperature observations confirmed deep-ocean observations (Garrett and Munk, 1972) that

$$P_{KE}(\sigma) \approx P_{PE}(\sigma) \approx P(\sigma) \propto N\sigma^{-2} \quad (9)$$

for $f \ll \sigma \ll N$

expressing equipartition of energy within the internal gravity wave band.

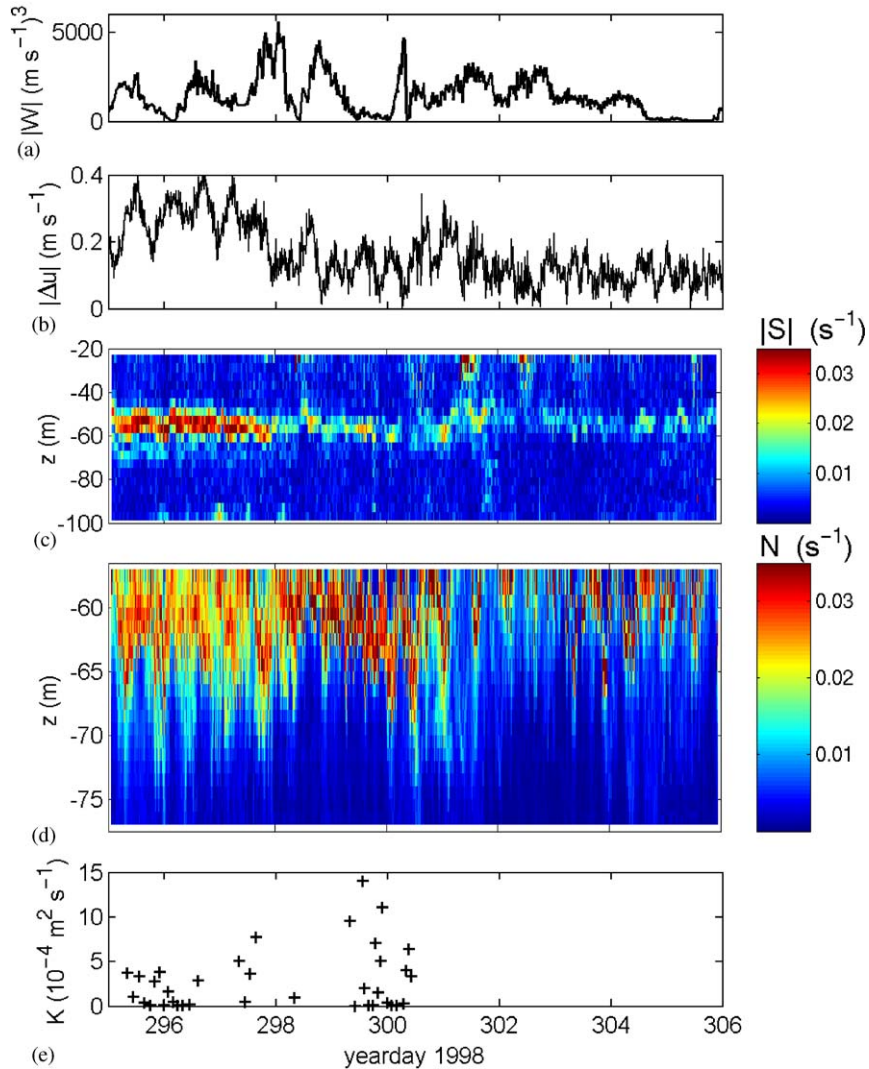


Fig. 4. Details of autumnal shear and stratification observed in the northern North Sea. (a) Wind speed cubed measured at Frigg. (b) Unsmoothed velocity difference between $z = -85$ and -30 m measured by 150 kHz ADCP. This velocity difference across stratification is largely due to inertial motions, which appeared mainly in a mode-1 vertical structure. (c) Unsmoothed shear magnitude computed using 4 m binned 150 kHz ADCP data (sub-sampled every third data point for limited filesize). (d) Unsmoothed stratification computed from fast thermistor string data using Eq. (4) (sub-sampled every 5 min for limited filesize). Around day 298 the relatively thick pycnocline becomes thinner and darker red (stronger stratification). Although the pycnocline occasionally rises outside the window after day 300, further stratification intensification and pycnocline thinning is seen later from the increasingly darker red colouring (with large excursions e.g. around days 303–304). (e) Eddy diffusivity inferred from 42 raw (24 Hz)-CTD observations near the moorings using Eq. (5) with N_m at the edges of the pycnocline $z = (z_b, z_s)$ in Eq. (6).

For $\sigma \gg N_A$ the observed enhancement of the spectral level by a factor $1/(0.45)^2$ was entirely attributable to scaling. The *displacement* spectra remained unchanged at these super-buoyancy

frequencies. This apparent temperature ‘noise’ was closely related to variations with time of ‘background’ stratification, possibly to Doppler-shifted high-frequency internal waves and/or

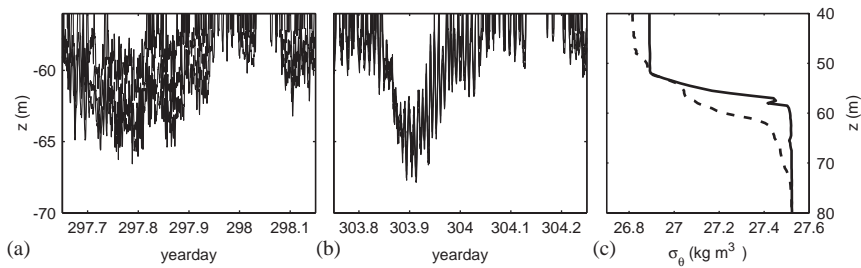


Fig. 5. (a, b) Unsmoothed detailed (30 s data) time series of unsmoothed pycnocline core of three isotherms at 0.5°C intervals (the three isotherms merge most of the time in panel (b)). Note the large difference in pycnocline thickness between the two panels, accompanied by very high-frequency (noise-like) pycnocline motions in (a) and regular large-amplitude waves in (b). (c) Two examples of 0.5 m vertically averaged density anomaly profiles with depth from CTD near the moorings. Dashed profile obtained at day 294.6, solid profile at day 300.0 (just prior to suspension of CTD observations).

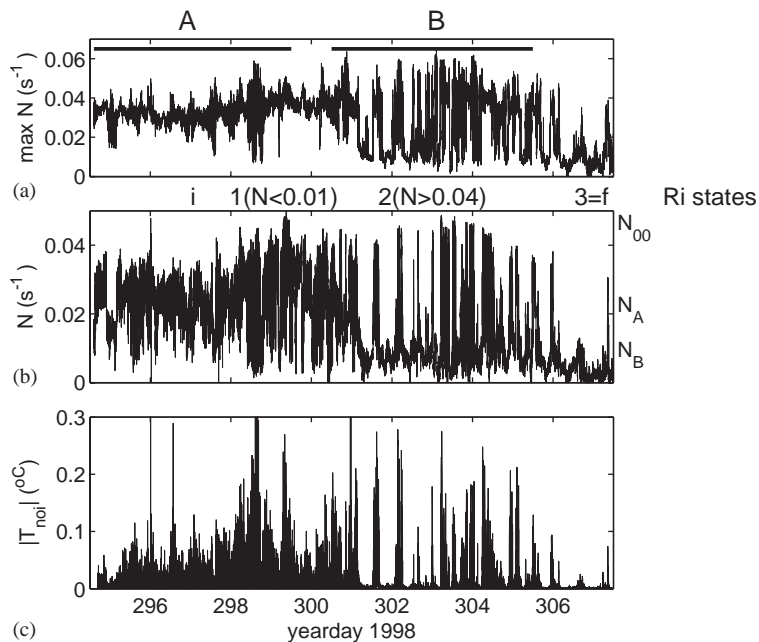


Fig. 6. (a) Unsmoothed (30 s data) time series of maximum buoyancy frequency per time step. (b) Unsmoothed (30 s data) time series of buoyancy frequency computed around $z = -61$ m from two neighbouring fast thermistors. Note the transition commencing around day 298 from a single mean value for buoyancy frequency to a much wider range focusing on two new mean values after day 300.5. (c) Temperature ‘noise’ (30 s) data at $z = -61$ m, defined as the high-frequency signal remaining after applying a very high-pass filter with cut-off at $3.5 \times 10^{-2} \text{ s}^{-1}$.

overturning events (Thorpe, 1987), while well-exceeding instrumental noise. Therefore, as it represented high frequency internal waves in the pycnocline it adopted the familiar internal wave spectral slope in Eq. (9). Likely, it represented

evanescent waves as we observed in low-stratification well outside the thermocline.

As a result, we ‘observed’ apparent *weakening* of the pycnocline as inferred from macro-observations like decreases in internal wave band energy

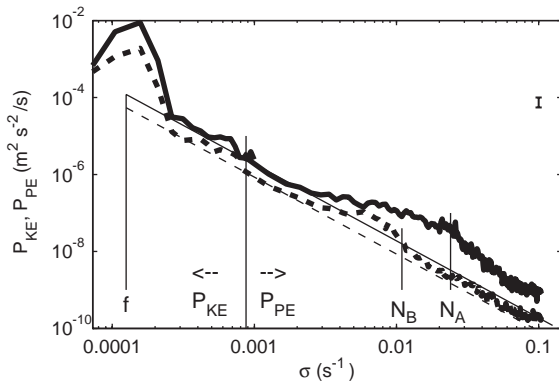


Fig. 7. Observed internal wave band spectra of kinetic energy (P_{KE} ; near the inertial frequency f) and potential energy (P_{PE} near the buoyancy frequencies N_A , N_B). P_{KE} and P_{PE} -spectra reach to $9 \times 10^{-4} \text{ s}^{-1}$, P_{KE} for $\sigma < 9 \times 10^{-4} \text{ s}^{-1}$ and P_{PE} for $\sigma > 9 \times 10^{-4} \text{ s}^{-1}$. The former are from 4 m binned 150 kHz ADCP measurements. The latter are computed using 7.700°C and 8.400°C -isotherm displacement data within the thermocline around $z = -61 \text{ m}$ interpolated from the fast thermistor string data for periods A (days 294.6–299.6) and B (300.5–305.5), respectively. Spectra are shown for data pieces of 5 days. The solid lines represent period A, dashed lines B (cf. Fig. 6 for periods). In the P_{PE} spectra, clearly the reduction of N with time ($N_B < N_A$) can be seen from the shift towards lower frequency of the enhancement above the continuum level (σ^{-2} -slope) near N . This N -reduction is also visible in both P_{KE} and P_{PE} -spectra for $f \ll \sigma \ll N$, where energy is smaller by a factor N_B/N_A during the second period, with respect to the first. (This is inferred from the straight-line model slopes representing σ^{-2} fall-off rate and which are off-set by N_B/N_A .) Note that for $\sigma > N_A, N_B$ the P_{PE} spectra do not ‘obey’ N -scaling, while the corresponding displacement spectra P_η are identical at these frequencies.

and current and temperature differences across stratification, while *enhancement* of stratification in a thinned layer. For an explanation (of the latter, new observation) we considered the dynamic stability balance.

5. Richardson number balance

The observed collapse of shear, followed by thinning of the pycnocline while stratification increased, can be interpreted using a Richardson number concept. Rewriting Eqs. (1)–(3) in terms of finite differences (Δ) gives

$$Ri(z, t) = \frac{-g}{\rho} \frac{\Delta\rho}{\Delta u^2 + \Delta v^2} \Delta z \quad (10)$$

indicating the importance of the vertical length scale over which the density and current vary.

Linden (1979) explored this importance from laboratory experiments. He inferred the relative amount of mixing across a pycnocline from the relative thickness of density and current interfaces. Mixing inside an interface by, for example, Kelvin–Helmholtz instability results in a thicker interface as kinetic energy was released from the current field (see also laboratory model results by Thorpe, 1971). Consequently, when an interface becomes thinner after a mixing event an ‘additional turbulent source is needed’ (Linden, 1979). In that case, the water column tends to be more stable after the event. This is understood by rewriting Eq. (10) in terms of the interface thicknesses of density (d_ρ) and current change (d_u). In the case that the current interface remains unaltered and the density interface thickness becomes smaller between the initial (subscript i) and the final (subscript f) state some time later, $d_{\rho f} < d_{\rho i}$, the Richardson number increases with time between these states

$$Ri_f = Ri_i d_{uf}^2 / (d_{\rho f} d_i) \quad (d_{ui} = d_{\rho i} = d_i) \\ > Ri_i \quad (11)$$

and the stratification becomes super-stable after an initially marginally stable state. This would sufficiently explain the observed transition $N_A \rightarrow N_{00}$ in Fig. 6, but the reality is more complex as will be outlined step-by-step below.

Starting the Richardson number interpretation (10) and (11) of our observations just prior to passage of the atmospheric disturbance on day 297.5–298.0, we had (Knight et al., 2002; van Haren et al., 2003),

$$Ri_i = \frac{-g}{\rho} \frac{(\Delta_d \rho)_i}{(\Delta_d U)_i^2} d_i \approx 0.5 - 1, \quad (12)$$

where Δ_d denotes a finite difference across a layer of thickness d (short for d_ρ and d_u). The notation for shear is shortened to $(\Delta_d U)^2 = (\Delta_d u)^2 + (\Delta_d v)^2$. Now we follow Ri_j , for states $j = 1, 2, 3$ between the initial state i and final state f.

During the wind stress increase (Fig. 4a) and cyclonic rotation of the wind (Knight et al., 2002), the observed first change in any of the parameters in Eq. (12) was a drop in the (inertial) vertical

current difference on day 297.85 (Fig. 4b):

$$(\Delta_d U)_1 = (0.45 \pm 0.05)(\Delta_d U)_i.$$

This change implied an associated Richardson number that was super-stable, since the density interface did not change immediately

$$Ri_1 = 5 \pm 1 Ri_i \gg 1. \quad (13)$$

Then, within one inertial period $t < T_f = 2\pi/f$ two new equilibria (changes two and three) of marginal dynamical stability were formed. The second change in parameters of Eq. (12) was pycnocline thinning (Figs. 4d and 5) as followed from computing mean thickness (6) in isotherm following coordinates for the pycnoclines in Fig. 5,

$$D_2 = (0.2 \pm 0.05)D_i = 1.2 \pm 0.2 \text{ m}$$

so that

$$Ri_2(D_2) \approx Ri_i. \quad (14)$$

The third change in parameters of Eq. (12) was the small reduction in temperature difference $(\Delta_d T)_2 \approx 0.8(\Delta_d T)_i$ (Fig. 3d). As a result

$$N_2(D_2) \equiv N_{00} = (2 \pm 0.2)N_A, \quad (15)$$

corresponding very well to the observations in Fig. 6. This enhanced static stability supported higher frequency internal waves as observed in the temperature noise time series (Fig. 6c), albeit in a layer of reduced thickness only (van Haren et al., 2001). Average potential energy spectra (Fig. 7) did not reveal this as a spectral peak, which suggested that such peaks (near N) were determined by the larger scale environment.

Occasionally, this larger scale environment supported large waves (Figs. 4d and 5b). Then, the super-stable stratification was moved up and down the water column by interfacial displacements at $\sigma = N_3 \ll N_{00}$ up to crest–trough amplitudes $\eta_3 \approx 1.5D_i \approx 1.5\eta_i$ (Fig. 5). Using $P_\eta(\sigma) \propto \eta^2 \propto N^{-1}$ we find

$$N_3(\eta_3) \equiv N_B \approx (1/1.5)^2 N_A \approx N_A/2.25. \quad (16)$$

This ties very well in with Eq. (7) and with the observations in the energy spectra (Fig. 7). It also

implies (again) attaining the marginal dynamical stability equilibrium

$$Ri_3(\eta_3) \equiv Ri_f \approx Ri_i. \quad (17)$$

As a result, the dichotomy in stratification $N_A \rightarrow (N_{00}, N_B)$ implied the possibility of support of very high-frequency internal gravity waves at frequencies $N_B (< N_A) < \sigma < N_{00}$ in a relatively thin wave guide D_2 , while the overall highest possible frequency for linear waves was set by the overall (large-scale) shear $|S|_B \approx N_B$.

6. Discussion

The present detailed observations from the autumnal Northern North Sea demonstrated the influence of high-frequency internal gravity waves on the control of the buoyancy frequency variation and overall internal wave scaling. So far, we have not considered its effects on diapycnal mixing during this short period when external (boundary) mixing did not dominate autumnal erosion of N . Internal waves near the buoyancy frequency just filled the enhanced vertical extent of reduced large-scale inertial shear: the background wave guide. The super-stable thin layer (Fig. 5) moving in a thicker shear layer was expected to be very stable, according to Eq. (11) and the discussion by Linden (1979). Our observations showed that a super-stable state did not last long, and a dynamical marginal stable state was reached within one inertial period by the filling of the (reduced) shear layer by displacement (‘mode-1’) waves (Fig. 1b(iii)). This confirmed earlier findings (Eriksen, 1978), including significant internal wave energy at $\sigma > N$, attributed by Eriksen (1978) to evanescent waves. We expected further reduction of stratification due to breaking on the edges of the wave guide, as an addition to boundary mixing, thus combining all three mechanisms (i)–(iii) in Fig. 1b.

Although our CTD-sampling was not exhaustive, cf. Eq. (4), we estimated eddy diffusivity values using Eq. (5) within the pycnocline: $K(z) = 1 - 10 \times 10^{-4} \text{ m}^2 \text{ s}^{-1}$, $z_b < z < z_s$ (Fig. 4e); due to occasional overturns at the edges of, but within, the pycnocline (Fig. 5c). These values, observed during short periods only, were about a decade

larger in magnitude than observed in summer (van Haren et al., 1999). Eventually, this (short-term) mixing may have eroded the thin layer stratification as well, after the near- N -waves reached maximum amplitudes around day 304 and N_{00} decreased (Fig. 6). Further evidence of such ‘internal’ mixing was not observed, and apparently mixed water was redistributed along isopycnal surfaces as no heating of the bottom boundary layer was observed during the (limited) period of observations. We noted that this internally driven mixing also occurred during low atmospheric-induced turbulence (Fig. 3a). Our observations were different from inertial-current-induced mixing events as described by Krauss (1981) and van Haren (2000), because the pycnocline thinned instead of thickened.

Pycnocline thinning in association with an increase in the bottom boundary layer was also observed in the shallower central North Sea after the passage of an autumnal storm (Fig. 8). This pycnocline thinning was not associated with a frontal passage as the pycnocline remained near mid-depth after the event. Compared to the northern North Sea data these observations had a higher vertical ($\Delta z = 0.5$ m) and temporal ($\Delta t = 1$ min) resolution of shear and equal vertical ($\Delta z = 1$ m) and less temporal ($\Delta t = 2$ min) resolution of stratification. Despite the high resolution, shear was observed to follow the (thin) layer of enhanced stratification strictly on the time scale of several hours, indicating the dominance of tidal and inertial quasi-circular shear. However, the observed enhancement of the bottom boundary layer and the apparent tidal-inertial oscillation of shear and stratification were caused by a somewhat different mechanism than the overall decrease of inertial shear magnitude in the northern North Sea. In the central North Sea, the frequency of the shear *magnitude* changed, implying a dramatic change from its slow modulation, inherent to quasi-circular shear (for instance varying on the spring–neap cycle). The initially slow modulation of $|S|$, with shear components varying at near-inertial scales and in equilibrium Eq. (12), became distorted when circular shear was superposed on shear at a different frequency, in this case as direct wind-induced shear. Hence, the shear magnitude

became a relatively fast varying function of time (and space), also varying at the near-inertial scale. During each moment of minimal shear in the near-inertial cycle the pycnocline thinned (Fig. 8c). This was observed only once in the northern North Sea. This explained the increase of the bottom boundary layer and shear, which reached maximum values at day 223.7 after which the now familiar dichotomy of higher and lower N was observed, and the overall current difference decreased.

Although the precise mechanism for growth of high-frequency internal waves is beyond our scope here, requiring future investigations, straining following shear modulation is a possibility. Another suggestion is the input of atmospheric energy. This may be communicated into the interior through the interaction of two surface waves propagating in nearly opposing directions (Thorpe, 1966), while energetic enough to reach the pycnocline at some 50 m depth. Alternatively, such deep penetration could be achieved through near-inertial waves feeding directly high-frequency internal waves by nonlinear interaction within the internal wave band itself. High-resolution observations from the pycnocline in the Mediterranean Sea by Woods (1968) and in the Sargasso Sea by Marmorino (1987) and Marmorino et al. (1987) showed breaking of high-frequency internal waves in the latter area associated with passages of near-inertial waves. Some evidence for this was found in a displacement spectrum around the period of the largest waves near the buoyancy frequency observed in the northern North Sea (Fig. 9). This spectrum showed a gap at intermediate internal wave frequencies with respect to the canonical internal wave fall-off rate (Garrett and Munk, 1972), while peaks near f (inertial-tidal frequencies) and N approximately had the same variance. Open ocean internal wave models showed near N waves generated by scattering of internal tidal waves off a thermocline, via solitary wave generation (Gerkema, 2001).

7. Conclusions

We have studied pycnocline behaviour during the autumnal breakdown of stratification. As

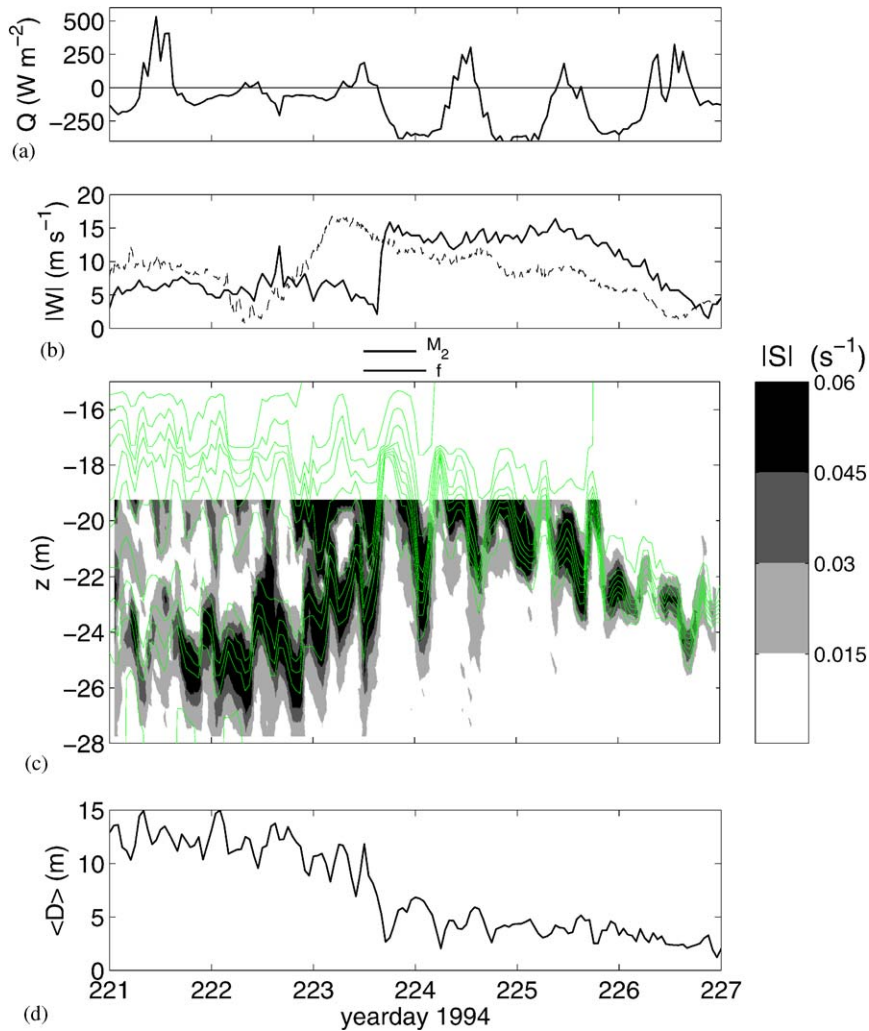


Fig. 8. Details of autumnal shear and stratification observed in the central North Sea. (a) Net radiation measured at a meteorological buoy at INP. (b) Wind speed measured at F3 (solid) and K13 (dashed), showing typical variations of about 0.5 day over the distance of about 300 km between the rigs. (c) Shear (shaded) from 0.5 m vertical binned data obtained using 1.2 MHz ADCP suspended in a mooring line, which also supported a standard Aanderaa thermistor string providing data on stratification (isotherms) from 1 m vertically separated sensors. During the passage of a storm on days 223/224, the isotherms (green lines at 1°C intervals) first moved upward and straining increased. (d) Pycnocline thickness computed using Eq. (6).

observed previously, atmospheric boundary mixing reduced the near-surface temperature steadily with time. When inertial currents were generated internal mixing occurred via large-scale inertial shear. In contrast with previous observations we showed for the first time occasionally very large high-frequency internal gravity waves supported by a very stable and thin interface, following the

collapse of inertial shear after the passage of an (out-of-phase) storm.

The interpretation of the counter-intuitive increase of pycnocline stability following an autumn storm was given in terms of marginal dynamical (Richardson number) stability. This fitted all of the observed variables on temperature (density) stratification, current and shear. Analysis in

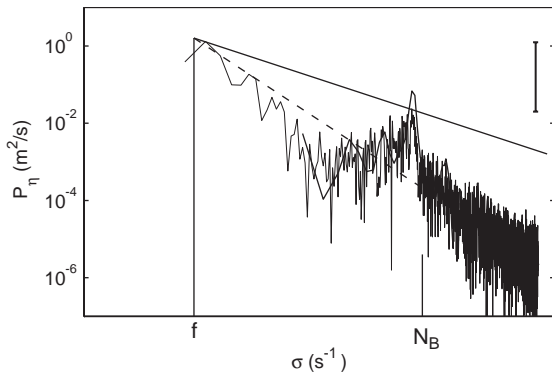


Fig. 9. Nearly raw (~ 3 degrees of freedom) displacement spectrum of 1.4 days of 8.400°C -isotherm data inferred from fast thermistor string data obtained in the northern North Sea between days 303.3 and 304.7, when background $N = N_B$. The overlaid peak near N is the spectrum between days 303.8 and 304.1. The dashed line indicates σ^{-2} -slope, the solid line σ^{-1} -slope.

isotherm following coordinates using high-resolution instrumentation revealed that sparsely sampled free internal waves and evanescent waves caused the ‘internal wave band spectrum’ to extend to frequencies higher than the ‘background’ N . These motions were not due to finestructure contamination. Background- N was caused by near- N waves just filling the layer of large-scale shear, after shear magnitude had dropped suddenly. This shear was found predominantly at low-frequency internal wave frequencies near f so that its vector described a circular path and its magnitude was varying at sub-inertial timescales. The shear accommodated a marginal stability criterion, so that large shear limited high-frequency internal wave growth: largest near- N waves were observed after the shear was reduced.

Our observations suggested that (‘buoyancy’)-scaling of equilibrium internal wave band energy was better in terms of $|S|$ than in terms of N , as the former were predominantly generated by large-scale low-frequency internal waves. This confirmed straining studies by Pinkel (1981). In other words, the energetics of a saturated internal wave field was best dominated by a constant background shear, modified slightly by straining of stratification. It is clear from the present observations that future studies require high vertical resolution of

current (shear) measurements in conjunction with high-resolution density (temperature measurements) to study the relevant processes across a pycnocline.

Acknowledgements

We enjoyed the assistance of the crews of R/V Pelagia and R/V Challenger. We thank Toby Sherwin for critically commenting a previous draft of this paper. Processes of Vertical Exchange in Shelf Seas (PROVEX) is a MAST3 project funded in part by the Commission of the European Communities Directorate General for Science and Education, Research and Development under Contract #MAS3-CT97-0159. The Integrated North Sea Program (INP) was funded in part by the Netherlands Organization for the advancement of Scientific Research (NWO).

Appendix A. Thickening of the bottom boundary layer below a pycnocline

The observed thickening of the near-bottom boundary layer above the tidal frictional height can be attributed to two effects. Both effects are associated with atmospheric forcing, but do not require well-mixed conditions throughout the water column, since the pycnocline was not (yet) destroyed.

The first effect was direct through the generation of a (surface) wave bottom boundary layer. Considering the large water depth ($H = 110$ m), this effect was only large near the end of the record, when atmospheric forcing was relatively large (Fig. 3a). Although a surface wave bottom boundary layer is usually very thin (~ 1 m typically), shear is very high and turbulence production is. (Speculating) this turbulence may be transported vertically upwards, perhaps by the strong vertical motions associated with surface waves, thereby modifying the tidal boundary. The second effect was indirect through near-inertial motions, generating largest shear across the pycnocline following ‘barotropic’ generation and coastal boundary condition (Millot and Crépon,

1981), and under certain turbulence conditions also in the near-bottom layer (Maas and van Haren, 1987). Theoretically, in steady state, a frictional-rotation balance (Ekman dynamics) does not apply for inertial motions, as the (anticyclonic) frictional boundary layer $\delta_- = \sqrt{(2A/|\sigma - f|)}$, A denoting a constant eddy viscosity, becomes infinitely thick when $\sigma \rightarrow f$. This expresses the sensitivity of (near-) inertial motions to turbulence. However, a tractable situation occurs when low-frequency relative vorticity is nonzero, and a near-inertial frictional boundary larger (smaller) than a tidal boundary layer is expected when horizontal current differences are smaller (larger) than $O(10^{-5} \text{ s}^{-1})$. Such values for low-frequency vorticity are not uncommon (Maas and van Haren, 1987; Knight et al., 2002).

References

- Bouruet-Aubertot, P., Thorpe, S.A., 1999. Numerical experiments on internal gravity waves in an accelerating shear flow. *Dynamics of Atmosphere-Oceans* 29, 41–63.
- Brainerd, K.E., Gregg, M.C., 1995. Surface mixing and mixing layer depths. *Deep-Sea Research I* 42, 1521–1543.
- Burchard, H., Bolding, K., Rippeth, T.P., Stips, A., Simpson, J.H., Sündermann, J., 2002. Microstructure of turbulence in the northern North Sea: a comparative study of observations and model observations. *Journal of Sea Research* 47, 223–238.
- Eriksen, C.C., 1978. Measurements and models of fine structure, internal gravity waves, and wave breaking in the deep ocean. *Journal of Geophysical Research* 83, 2989–3009.
- Garrett, C.J.R., Munk, W.H., 1972. Space-time scales of internal waves. *Geophysical Fluid Dynamics* 3, 225–264.
- Gerkema, T., 2001. Internal and interfacial tides: beam scattering and local generation of solitary waves. *Journal of Marine Research* 59, 227–255.
- Howarth, M.J., Simpson, J.H., Sündermann, J., van Haren, H., 2002. Processes of vertical exchange in shelf seas (PRO-VESS). *Journal of Sea Research* 47, 199–208.
- Knight, P.J., Howarth, M.J., Rippeth, T., 2002. Inertial currents in the northern North Sea. *Journal of Sea Research* 47, 269–284.
- Krauss, W., 1981. The erosion of the pycnocline. *Journal of Physical Oceanography* 11, 415–433.
- Linden, P.F., 1979. Mixing in stratified fluids. *Geophysical and Astrophysical Fluid Dynamics* 13, 3–23.
- Maas, L.R.M., van Haren, J.J.M., 1987. Observations on the vertical structure of tidal and inertial currents in the central North Sea. *Journal of Marine Research* 45, 293–318.
- Marmorino, G.O., 1987. Observations of small-scale mixing processes in the seasonal thermocline. Part II: wave breaking. *Journal of Physical Oceanography* 17, 1348–1355.
- Marmorino, G.O., Rosenblum, L.J., Trump, C.L., 1987. Fine-scale temperature variability: the influence of near-inertial waves. *Journal of Geophysical Research* 92, 13,049–13,062.
- Miles, J., 1987. Richardson's number revisited. In: *Preprints of Third International Symposium on Stratified Flows*, CalTech, Pasadena, CA, February 3–5, pp. 1–7.
- Millot, C., Crépon, M., 1981. Inertial oscillations on the continental shelf of the Gulf of Lions—observations and theory. *Journal of Physical Oceanography* 11, 639–657.
- Munk, W., 1981. Internal waves and small-scale processes. In: Warren, B.A., Wunsch, C. (Eds.), *Evolution of Physical Oceanography*. MIT Press, Cambridge, MA, pp. 264–291.
- Munk, W.H., Anderson, E.R., 1948. Notes on a theory of the thermocline. *Journal of Marine Research* 7, 276–295.
- Pinkel, R., 1981. Observations of the near-surface internal wave field. *Journal of Physical Oceanography* 11, 1248–1257.
- Pollard, R.T., Millard Jr., R.C., 1970. Comparison between observed and simulated wind-generated inertial oscillations. *Deep-Sea Research A* 17, 813–821.
- Pollard, R.T., Rhines, P.B., Thompson, R.O.R.Y., 1973. The deepening of the wind-mixed layer. *Geophysical Fluid Dynamics* 3, 381–404.
- Thorpe, S.A., 1966. On wave interactions in a stratified fluid. *Journal of Fluid Mechanics* 24, 737–751.
- Thorpe, S.A., 1971. Experiments on the instability of stratified shear flows: miscible fluids. *Journal of Fluid Mechanics* 46, 299–319.
- Thorpe, S.A., 1987. Current and temperature variability on the continental slope. *Philosophical Transactions of the Royal Society of London A* 323, 471–517.
- Turner, J.S., 1973. *Buoyancy Effects in Fluids*. Cambridge University Press, Cambridge, MA, 368 pp.
- Turner, J.S., Krauss, E.B., 1967. A one-dimensional model of the seasonal pycnocline. I. A laboratory experiment and its interpretation. *Tellus* 19, 88–97.
- van Haren, H., 1996. Correcting false thermistor string data. *Continental Shelf Research* 16, 1871–1883.
- van Haren, H., 2000. Properties of vertical current shear across stratification in the North Sea. *Journal of Marine Research* 58, 465–491.
- van Haren, H., Maas, L., Zimmerman, J.T.F., Ridderinkhof, H., Malschaert, H., 1999. Strong inertial currents and marginal internal wave stability in the central North Sea. *Geophysical Research Letters* 26, 2993–2996.
- van Haren, H., Groenewegen, R., Laan, M., Koster, B., 2001. A fast and accurate thermistor string. *Journal of Atmospheric and Oceanic Technology* 18, 256–265.
- van Haren, H., Howarth, M.J., Jones, K., Ezzi, I., 2003. Autumnal reduction of stratification in the northern North Sea. *Continental Shelf Research* 23, 177–191.
- Woods, J.D., 1968. Wave-induced shear instability in the summer thermocline. *Journal of Fluid Mechanics* 32, 791–800.